

Resistive switching memory effect of ZrO_2 films with Zr^+ implanted

Qi Liu, Weihua Guan, Shibing Long, Rui Jia, and Ming Liu^{a)}

Laboratory of Nano-fabrication and Novel Devices Integrated Technology, Institute of Microelectronics, Chinese Academy of Sciences, Beijing 100029, People's Republic of China

Junning Chen

College of Electronics and Technology, Anhui University, Hefei 230039, People's Republic of China

(Received 6 November 2007; accepted 17 December 2007; published online 10 January 2008)

The $\text{Au}/\text{Cr}/\text{Zr}^+\text{-implanted-}\text{ZrO}_2/n^+\text{-Si}$ sandwiched structure exhibits reversible bipolar resistive switching behavior under dc sweeping voltage. The resistance ratio (R_{ratio}) of high resistive state and low resistive state is as large as five orders of magnitude with 0.5 V readout bias. $\text{Zr}^+\text{-implanted-}\text{ZrO}_2$ films exhibit good retention characteristics and high device yield. The impact of implanted Zr^+ ions on resistive switching performances is investigated. Resistive switching of the fabricated structures is explained by trap-controlled space charge limited current conduction. © 2008 American Institute of Physics. [DOI: 10.1063/1.2832660]

While traditional memories are approaching their scaling limits, the next generation nonvolatile memory has attracted extensive attention. One of the promising candidates is the resistive random access memory (RRAM) due to its superior characteristics including simple structure, high density integration, low power consumption, and fast write/erase operation. The current candidate materials for RRAM devices include ferromagnetic material,¹ organic material,² doped perovskite,³ and binary oxides such as NiO ,⁴ TiO_2 ,⁵ Al_2O_3 ,⁶ SiO_2 ,⁷ and Cu_xO .⁸ Although various models for resistive switching have been suggested, e.g., formation and rupture of metallic filament,⁹ Schottky barriers with interface states,¹⁰ electrochemical migration at the interface,¹¹ and trap charging and discharging,¹² the exact switching mechanism has not yet clearly understood. Recently, Lee *et al.* reported the resistive switching behavior of nonstoichiometric zirconium oxide (ZrO_x).¹³ Wu *et al.* further presented a possible way to improve the device yield by replacing nonstoichiometric ZrO_x with stoichiometric ZrO_2 .¹⁴ Our previous study indicated that the intentionally introduced external traps in ZrO_2 films can significantly improve the device yield due to more uniform and homogeneous trap concentrations.¹⁵

In this letter, we utilize the ion implantation techniques to fabricate the $\text{Au}/\text{Cr}/\text{Zr}^+\text{-implanted-}\text{ZrO}_2/n^+\text{-Si}$ structures. The reversible bipolar resistive switching behavior of $\text{Zr}^+\text{-implanted-}\text{ZrO}_2$ thin films are observed. The physical origin of this switching phenomenon is also suggested.

The resistive switching memory devices are prepared through the following processes. First, n^+ silicon wafer ($3.5 \times 10^{-3} \Omega \text{ cm}$) are cleaned by $\text{H}_2\text{SO}_4/\text{H}_2\text{O}_2$ and $\text{HF}/\text{H}_2\text{O}$ (1:7) solutions, rinsed with de-ionized water, and dried in N_2 . Second, a 70-nm-thick ZrO_2 film is deposited by electron beam evaporation at a base pressure of 2.6×10^{-6} Torr. The deposition rate for ZrO_2 film is 1 Å/s . After that, Zr^+ is implanted into the ZrO_2 film with $3 \times 10^{12} \text{ cm}^{-2}$ dose and 70 KeV energies. In order to crystallize ZrO_2 and activate Zr^+ ions, $\text{Zr}^+\text{-implanted-}\text{ZrO}_2$ film is annealed at 800°C for 30 s in N_2 ambient (2.5 L/min). Finally, the top electrodes of 10-nm-thick Cr and 50-nm-thick

Au are evaporated. All the top electrodes are defined to square shape with side length ranging from 50 to $800 \mu\text{m}$ by the lift-off process. To investigate the role of the implanted Zr^+ in resistive switching phenomenon, control samples without Zr^+ implantation is simultaneously fabricated. Keithley 4200 semiconductor characterization system is used to measure the current-voltage (I - V) characteristics of the fabricated devices.

Figure 1 shows the plot of current versus bias voltage of $\text{Au}/\text{Cr}/\text{Zr}^+\text{-implanted-}\text{ZrO}_2/\text{Si}$ structures (denoted as implanted samples) and $\text{Au}/\text{Cr}/\text{ZrO}_2/\text{Si}$ structures (denoted as un-implanted samples). By sweeping the voltage ($0 \rightarrow 4 \rightarrow 0 \rightarrow -4 \rightarrow 0 \text{ V}$), the typical I - V characteristic of the implanted samples is observed with a conspicuous I - V hysteresis. While positive voltage is applied on the top electrode, the current rapidly increases at V_{set} and the device switches from the off state to the on state. Then, the state holds on the low resistive state (LRS) after sweeping the bias voltage from 4 to 0 V. The current increases with increasing bias voltage in the negative direction and the devices switch from on state to off state at V_{reset} voltage. Then the state holds on

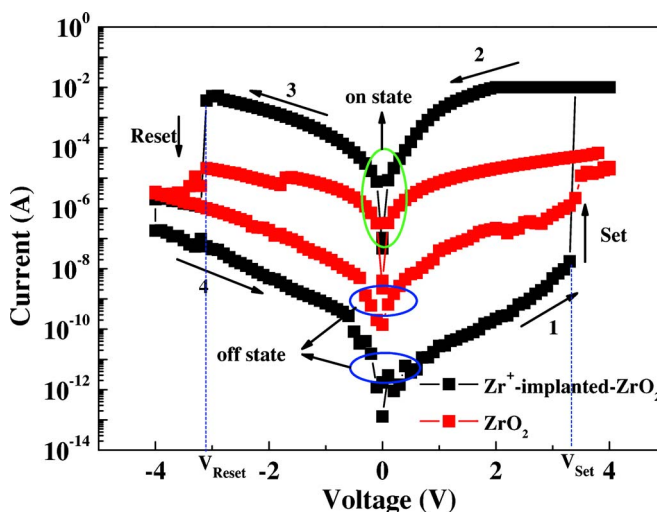


FIG. 1. (Color online) The typical I - V characteristics of the implanted samples and the unimplanted samples under voltage sweeping ($0 \rightarrow 4 \rightarrow 0 \rightarrow -4 \rightarrow 0 \text{ V}$).

^{a)} Author to whom correspondence should be addressed. Electronic mail: liuming@ime.ac.cn. Tel.: 86-10-62007699. FAX: 86-10-62055666.

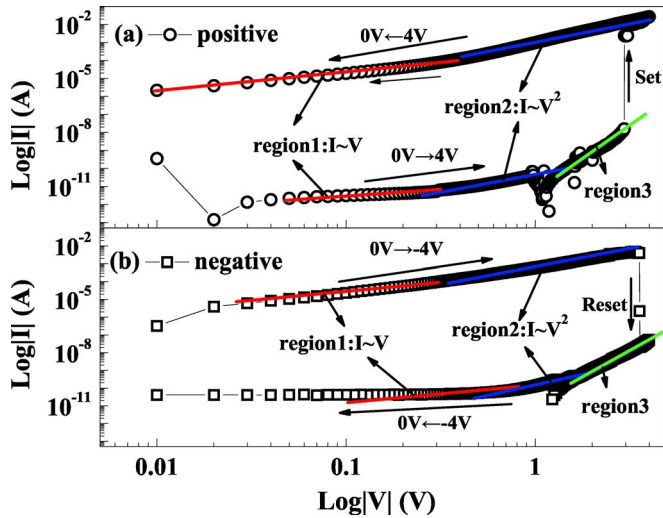


FIG. 2. (Color online) Replots the I - V characteristics of the implanted samples in log-log scale: (a) positive voltage region and (b) negative voltage region.

the high resistive state (HRS) after sweeping the bias voltage from -4 to 0 V. The typical I - V characteristic of the unimplanted samples is similar to that of the implanted samples. However, as can be seen in Fig. 1, the on state current of the implanted samples is higher than the unimplanted samples while the off state current of the implanted samples is lower than the unimplanted samples. The resistance ratio of the implanted samples is about five orders of magnitude, larger than that of the unimplanted samples. Moreover, we observed in the experiment that the device yield of the implanted samples is higher than the unimplanted samples.

To clarify the conduction mechanisms of the implanted samples, the I - V curve in the positive and negative voltage regions are replotted in a log-log scale in Figs. 2(a) and 2(b), respectively. As described in Ref. 16, the typical I - V characteristic of trap-controlled space charge limited current (SCLC) is constituted of three portions: the Ohmic region ($I \sim V$), the child's square law region ($I \sim V^2$), and the steep increase in current region. Our observed I - V curves, as shown in Fig. 2, are in good agreement with the prediction of trap-controlled SCLC. Within both the positive and negative voltage regions, the slopes of HRS and LRS are very close to linear in the low voltage region (region 1), which corresponds to the Ohmic law region. At voltage larger than 0.5 V, the current of both the HRS and LRS follows square dependence on voltage (region 2), corresponding to the child's square law region. In higher voltage region (>1 V), the current of HRS increases very fast (region 3), corresponding to the steep increase in current region.

The current density for trap-controlled SCLC emission can be expressed as follows:¹⁶

$$J = \left(\frac{\theta}{\theta + 1} \right) (9/8) \epsilon_r \epsilon_0 \mu \frac{V^2}{L^3},$$

where, J is the current density, $\theta = (N_C/N_t) \exp^{-(E_C - E_t)/kT}$ is the ratio of free electron to trapped electron, N_C is the effective density of states in the conductive band, N_t is the number of emptied electron traps, ϵ_0 is the permittivity of free space, ϵ_r is the static dielectric constant, μ is the electron mobility, V is the applied voltage and L is the film thickness.

When majority of electron traps are emptied ($\theta \ll 1$, HRS

branches), the current-voltage characteristics are dominated by the trap. In this case, the current density equation can be rewritten as

$$J = \theta (9/8) \epsilon_r \epsilon_0 \mu \frac{V^2}{L^3}.$$

When majority of electron traps are occupied ($\theta \gg 1$, LRS branches), in this case, the current density can be rewritten as

$$J = (9/8) \epsilon_r \epsilon_0 \mu \frac{V^2}{L^3}.$$

From these equations, we can explain the resistive switching phenomenon of the implanted samples. For simplification, we assume only Zr^{+} electron trap exists in the Zr^{+} -implanted- ZrO_2 film. In the low voltage region, the density of thermally generated free electrons inside the ZrO_2 films is greater than that of the injected electrons from electrode; the I - V correlation is dominated by Ohmic emission mechanism. When the voltage value is increased, the density of injected electrons gradually exceeds the equilibrium concentration in the film, so the current is dominated by the injected electrons.

In the positive voltage region, when the voltage value reaches the trap-filled-limit voltage (V_{TFL}), the injected electrons from electrode divide into two parts, one is free electrons and the other is occupied trap electrons. In this case, the concentration of free electrons is greatly reduced since many of the electrons fill empty trap sites and, therefore, do not contribute to current flow. When the voltage reaches the set voltage, all Zr^{+} traps have been occupied by electron. In this case, the current steep increases and the device switches from the HRS to the LRS. When the positive bias reduces from 4 to 0 V, a majority of injected electrons is free electrons because most of Zr^{+} trap has been occupied, the device has maintained low resistance state.

In the negative voltage region, the occupied trap will discharge the electrons. When the voltage reaches the reset voltage, electrons detrap from the most of occupied traps, the current reduces quickly and the device switches from LRS to HRS. When the negative voltage reduces from -4 to 0 V, a majority of Zr^{+} traps have been emptied, the device maintained HRS. According to our discussion above, we infer that the resistive switching behavior of the implanted samples is due to electron trapping and detrapping from Zr^{+} traps in the ZrO_2 film and the conduction is dominated by trap-controlled SCLC mechanism.

Figure 3 shows the retention performance of the implanted samples under 0.5 V reading voltage at room temperature. The readout of LRS and HRS is performed after applied positive (4 V) and negative (-4 V) voltage for a short time, respectively. Then the resistance of LRS or HRS is recorded at 0.5 V reading voltage with an interval. The reading of the resistance state is nondestructive, and no electrical power is needed to maintain the resistance within a given state (LRS or HRS). As can be seen in Fig. 3, the LRS and HRS resistances are kept stable for more than 2500 s, confirming the nonvolatile nature of the device.

In conclusion, the Au/Cr/ Zr^{+} -implanted- ZrO_2 / n^{+} -Si device is fabricated and investigated for nonvolatile memory applications. The implanted samples show good resistive switching behaviors. Moreover, it is found that the implanted

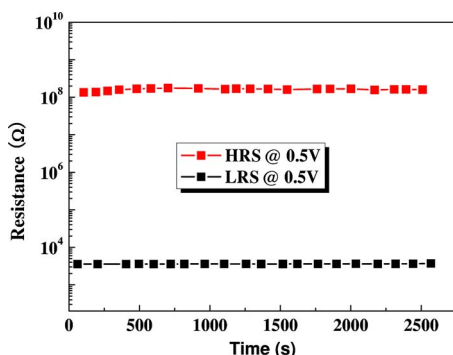


FIG. 3. (Color online) The retention characteristics of the implanted samples at room temperature. Both resistance of the HRS and LRS are kept stable over time of 2500 s.

samples exhibited larger resistive switching ratio and higher device yield than the unimplanted samples. The current of the implanted samples are governed by the trap-controlled SCLC conduction mechanism and the resistance switching is due to electron trapping and detrapping at Zr^{+} traps in ZrO_2 film.

This work is partly supported by National Basic Research Program of China (973 Program) under Grant No. 2006CB302706 and National Nature Science Foundation of China under Grant Nos. 90607022, 90401002, and 60506005.

- ¹S. Q. Liu, N. J. Wu, and A. Ignatiev, *Appl. Phys. Lett.* **76**, 2749 (2000).
- ²Y.-S. Lai, C.-H. Tu, D.-L. Kwong, and J. S. Chen, *Appl. Phys. Lett.* **87**, 122101 (2005).
- ³A. Beck, J. G. Bednorz, Ch. Gerber, C. Rossel, and D. Widmer, *Appl. Phys. Lett.* **77**, 139 (2000).
- ⁴D. C. Kim, S. Seo, S. E. Ahn, D.-S. Suh, M. J. Lee, B.-H. Park, I. K. Yoo, I. G. Baek, H.-J. Kim, E. K. Yim, J. E. Lee, S. O. Park, H. S. Kim, U.-In. Chung, J. T. Moon, and B. I. Ryu, *Appl. Phys. Lett.* **88**, 202102 (2006).
- ⁵C. Rohde, B. J. Choi, D. S. Jeong, S. Choi, J.-S. Zhao, and C. S. Hwang, *Appl. Phys. Lett.* **86**, 262907 (2005).
- ⁶K. M. Kim, B. J. Choi, B. W. Koo, S. Choi, D. S. Jeong, and C. S. Hwang, *Electrochem. Solid-State Lett.* **9**, G343 (2006).
- ⁷C. Schindler, S. C. P. Thermadam, R. Waser, and M. N. Kozicki, *IEEE Trans. Electron Devices* **54**, 2762 (2007).
- ⁸A. Chen, S. Haddad, Y. C. Wu, Z. Lan, T. N. Fang, and S. Kaza, *Appl. Phys. Lett.* **91**, 123517 (2007).
- ⁹B. J. Choi, D. S. Jeong, S. K. Kim, S. Choi, J. H. Oh, C. Rohde, H. J. Kim, C. S. Hwang, K. Szot, R. Waser, B. Reichenberg, and S. Tiedke, *J. Appl. Phys.* **98**, 033715 (2005).
- ¹⁰T. Fujii, M. Kawasaki, A. Sawa, H. Akoh, Y. Kawazoe, and Y. Tokura, *Appl. Phys. Lett.* **86**, 012107 (2005).
- ¹¹M. Mitkova, Y. Wang, and P. Boolchand, *Phys. Rev. Lett.* **83**, 3848 (1999).
- ¹²S. Seo, M. J. Lee, D. H. Seo, E. J. Jeoung, D.-S. Suh, Y. S. Joung, I. K. Yoo, I. R. Hwang, S. H. Kim, I. S. Byun, J.-S. Kim, J. S. Choi, and B. H. Park, *Appl. Phys. Lett.* **85**, 5655 (2004).
- ¹³D. S. Lee, H. J. Choi, H. J. Sim, D. H. Choi, H. S. Hwang, M.-J. Lee, S.-A. Seo, and I. K. Yoo, *IEEE Electron Device Lett.* **26**, 719 (2005).
- ¹⁴X. Wu, P. Zhou, J. Li, L. Y. Chen, H. B. Lv, Y. Y. Lin, and T. A. Tang, *Appl. Phys. Lett.* **90**, 183507 (2007).
- ¹⁵W. Guan, S. Long, R. Jia, and M. Liu, *Appl. Phys. Lett.* **91**, 062111 (2007).
- ¹⁶M. A. Lampert and P. Mark, *Current Injection in Solids* (Academic, New York, 1970).